

# Fully Controllable Structural Phase Transition in Thermomechanical Molecular Crystals with a Very Small Thermal Hysteresis

Yulong Duan, Sergey Semin, Paul Tinnemans, Jialiang Xu,\* and Theo Rasing\*

The construction of a practical crystalline molecular machine faces two challenges: to realize a collective molecular movement, and to amplify this movement into a precisely controlled mechanical response in real time and space. Thermosensitive single crystals display cooperative molecular movements that are converted to strong macroscopic mechanical responses or shape deformations during temperature-induced structural phase transitions. However, these collective molecular movements are hard to control once initiated, and often feature thermal hystereses that are larger than 10 °C, which greatly hamper their practical applications. Here, it is demonstrated that the phase boundaries of the thermomechanical molecular crystal based on a fluorenone derivative 4-DBpFO can be used to finely control its structural phase transition. When this phase transition is triggered at two opposite crystal faces, it is accompanied by two parallel phase boundaries that can be temperature controlled to move forward, backward, or to halt, benefitting from the stored elastic energy between the parallel boundaries. Moreover, the thermal hysteresis is greatly decreased to 2–3 °C, which allows for circular heating/cooling cycles that can produce a continuous work output.

Molecular crystals that undergo time-varying shape changes upon external stimuli are attractive for their potential applications as self-assembled molecular machines.<sup>[1]</sup> Compared to well-established shape change materials based on artificial polymers, gels, and liquid crystals,<sup>[2]</sup> the high elastic moduli, rapid response, and easily down-sizeable characteristics<sup>[3]</sup> make

these emerging dynamic crystals highly attractive. However, to create a crystalline molecular machine capable of tunable motions,<sup>[4]</sup> one has to realize an accurate cooperative molecular movement in the rigid solid crystals.<sup>[1b]</sup> More importantly, this molecular movement has to be converted into controllable macroscopic shape changes or motions in the desired time and space,<sup>[1d]</sup> similar to what happens in biological systems such as motor proteins.<sup>[5]</sup> Martensitic phase transitions<sup>[6]</sup> are displacive phase transitions involving the cooperative movement of many molecules, which could provide a new approach to the design of crystalline molecular machines.<sup>[7]</sup> A biological example for such a displacive phase transition was found in a protein crystal of T4 bacteriophage virus.<sup>[8]</sup> The tail sheath of the virus, which is a 2D protein crystal, shrinks via a martensitic phase transition, in order to puncture the bacterial membrane and to release the DNA of


the virus. Recently, this kind of phase transition has attracted extensive attention in thermosensitive molecular crystals, as the cooperative molecular movements can result in abrupt crystal shape changes that endows these crystals with pronounced mechanical responses and shape memory effects.<sup>[9,10]</sup>

However, to make thermosensitive crystals work as well-controllable micron-size crystalline machines, some crucial issues need to be addressed. First, theories<sup>[11]</sup> and experiments<sup>[10]</sup> both show that this type of phase transition is very fast, and the collective molecular movements can hardly be stopped or controlled once the phase transition is initiated.<sup>[11]</sup> Consequently, the thermosensitive crystals can usually only switch their shapes between the low-temperature (LT) phase and the high-temperature (HT) phase. Intermediate shapes, composed of a certain ratio of LT and HT phases, are often inaccessible. Therefore, the mechanical output, which is related to both crystal strain and strain rate, is hard to be quantitatively controlled. Second, the first-order nature of martensitic phase transitions<sup>[12]</sup> leads to large thermal hysteresis widths between the heating and cooling phase transition<sup>[13]</sup> (as large as 10–80 °C in reported thermomechanical crystals, **Table 1**). Such large thermal hystereses impede these crystals to achieve repeatable shape changes at a fast rate via circular heating/cooling cycles.

We have recently reported a martensitic-like phase transition between the  $\alpha$ -phase and the  $\beta$ -phase of the thermosensitive

Dr. Y. Duan, Dr. S. Semin, Dr. P. Tinnemans, Prof. T. Rasing  
Radboud University  
Institute for Molecules and Materials  
Heyendaalseweg 135, Nijmegen 6525AJ, The Netherlands  
E-mail: theo.rasing@ru.nl

Prof. J. Xu  
School of Materials Science and Engineering  
Nankai University  
Tongyan Road 38, Tianjin 300350, P. R. China  
E-mail: jialiang.xu@nankai.edu.cn

 The ORCID identification number(s) for the author(s) of this article can be found under <https://doi.org/10.1002/smll.202006757>.

© 2021 The Authors. Small published by Wiley-VCH GmbH. This is an open access article under the terms of the Creative Commons Attribution-NonCommercial-NoDerivs License, which permits use and distribution in any medium, provided the original work is properly cited, the use is non-commercial and no modifications or adaptations are made.

DOI: 10.1002/smll.202006757

**Table 1.** Thermal hysteresis widths between the forward (heating) and backward (cooling) phase transition temperatures of some thermosalient crystals.

Crystal	Forward transition temperature	Backward transition temperature	Temperature hysteresis width
[NiII(en) <sub>3</sub> ](ox) complex <sup>[1f]</sup>	270 K	251 K	≈19 K
Terephthalic acid <sup>[9b]</sup>	348–358 K	305–315 K	43 K
(Phenylazophenyl)palladium hexafluoroacetylacetonate ( $\alpha$ -phase to $\gamma$ -phase) <sup>[10]</sup>	342–355 K	325–306 K	30–36 K
Co-assembly of coronene and 1,2,4,5-tetracyanobenzene <sup>[9c]</sup>	26–49 °C	–51 to 34 °C	77–83 °C
Pyroglutamic acid <sup>[9d]</sup>			10–15 K
ditBu-BTBT <sup>[9e]</sup>	343–348 K	338–333 K	≈10 K

molecular crystal based on 2,7-di([1,1'-biphenyl]-4-yl)-fluorenone (4-DBpFO<sup>[14]</sup>) (**Figure 1**), which features clear coherent phase boundaries (Movie S1, Supporting Information). It appears that 4-DBpFO is the only reported thermosalient crystal so far that shows two different phase boundary directions in the same crystal during the phase transition. The crystal symmetry of the parent phase (orthorhombic) is higher than the produced phase (Monoclinic), so there will be two equivalent ways that the parent crystal can deform, and correspondingly there are two equivalent phase boundary directions during the low to high temperature phase transition. Moreover, the crystal side facets, (101), ( $\bar{1}0\bar{1}$ ), and (10 $\bar{1}$ ), which are also the phase boundary

planes, are symmetrically equivalent in the as-grown crystals. Therefore, the cooperative molecular displacements along these planes will consume the same amount of energy, which allows a crystal to have two or more phase boundaries at the same time. The different phase boundary directions offer the possibility to study how the phase boundary conditions, including single-, cross- and parallel-phase boundaries, can affect the thermodynamic properties of this type of phase transition. Actually, many theoretical and experimental investigations have been carried out to understand the thermal dynamic properties<sup>[15]</sup> and to control the movement of phase boundaries<sup>[16]</sup> in spin cross-over materials, which feature similar first-order cooperative

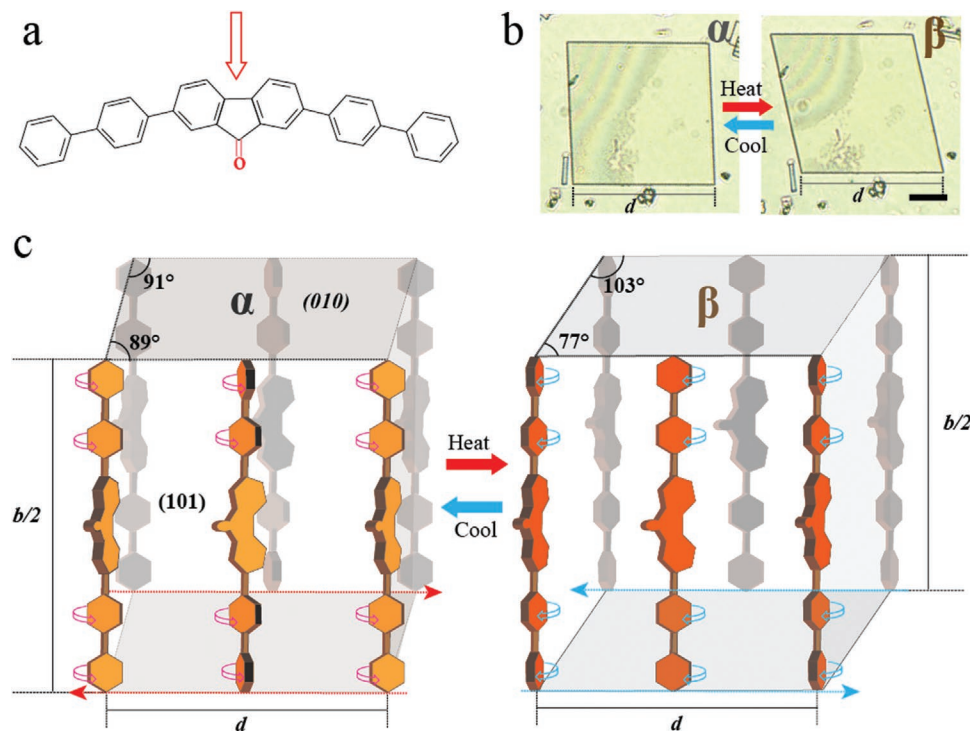


**Figure 1.** Structural phase transition of 4-DBpFO molecular crystal. a) The chemical structure of 4-DBpFO. The polar carbonyl group induces a permanent dipole (red arrow). b) Microscope images of the crystal shape deformation viewed from the (010) plane. Scale bar: 50  $\mu$ m. c) Illustration of the molecular dynamics during the structural phase transition. The collective in-plane rotation (round arrows) of the benzene rings results in an anisotropic lattice expansion in the (010) plane, generating a shear force (dashed linear arrows) that causes the cooperative linear molecular movement along the phase boundary. The side length,  $d$ , does not change during the phase transition. The normal cell length,  $b$ , does not change either, because the rotations of the benzene rings are in-plane. Note that the crystals have a layered molecular packing along the crystallographic  $b$ -axis. The linear dashed red and blue arrows show the directions of the cooperative molecular movements, while the round red and blue arrows show the directions of the benzene ring rotations upon heating and cooling, respectively.

phase transitions and mechanical responses<sup>[17]</sup> as those of thermosalient crystals. However, very few of these studies have been concerned with the phase boundary conditions such as their quantity and orientation.<sup>[18]</sup> Moreover, although the structural phase transition in thermosalient organic crystals is so significant that it may result in pronounced crystal shape deformation, crystal jumping and even crystal breaking/explosion,<sup>[9]</sup> the entropy variation at the structural phase transition point of thermosalient organic crystals can be very small. For example, the entropy change in thermosalient 4-DBpFO crystals ( $2.1\text{--}4.7\text{ J mol}^{-1}\text{ K}^{-1}$ ) is about 10 times smaller than that of typical spin cross over (SCO) materials ( $40\text{--}80\text{ J mol}^{-1}\text{ K}^{-1}$ ).<sup>[15d]</sup> This small entropy variation is consistent with the negligible crystal volume change ( $\approx 2.7\%$ ) during this order–order phase transition in spite of a large crystal shear strain ( $\approx 18\%$ ). Consequently, mechanisms in thermosalient materials can be related to but may not be exactly the same as in SCO materials. In this work, we report that thermodynamic properties such as the thermal hysteresis width, phase boundary moving speed and crystal integrity during the structural phase transition can be affected by the phase boundary conditions in 4-DBpFO thermosalient crystals. We demonstrate that the phase transition speed and crystal shape of 4-DBpFO can be well-controlled if the phase transition proceeds by parallel phase boundaries, benefiting from the elastic energy stored between them. Moreover, crystals transforming via parallel phase boundaries can return to their original shape within a very small temperature change of less than  $3\text{ }^{\circ}\text{C}$ , arising from the fact that the reversed phase transition does not require re-nucleation. These features not only provide new insights in the thermomechanics of martensitic phase transitions in molecular crystals, but also show the potential of 4-DBpFO as a time-varying and fast repeatable shape change material or controllable microcrystalline molecular machine.

The 4-DBpFO molecule contains one rigid fluorenone center with two phenyl planes linked by single bonds at each side (Figure 1a). The crystal structure of the  $\alpha$ -phase shows a layer by layer molecular packing which disfavors the formation of strong molecular forces between the layers (Figure S1, Supporting Information), and the relative in-plane rotation of the phenyl

planes can feasibly trigger the structural phase transition from the  $\alpha$ -phase (space group:  $Pnma$ ) to the  $\beta$ -phase (space group:  $P2_1/n$ ) (Figure 1c). The phase transition, which is accompanied by very clear coherent phase boundaries (Movie S1, Supporting Information), results in a major change in the corner angles of the rhomboidal shaped single crystals (with (010) basal planes and (101) or (10 $\bar{1}$ ) side faces), from  $89^{\circ}$  and  $91^{\circ}$  to  $77^{\circ}$  and  $103^{\circ}$ , respectively (Figure 1b). The change of the crystal corner angle is in line with the anisotropic in-plane crystallographic lattice expansion during the phase transition ( $a$ -axis changed from  $6.90$  to  $6.26\text{ }\text{\AA}$  and  $c$ -axis changed from  $7.27$  to  $7.77\text{ }\text{\AA}$ , respectively). Even though this shear deformation is very large, the normal direction of the crystals does not change as the phase transition only involves in-plane rotation of the phenyl planes (Figure 1c), which results in the excellent reversibility of the shape change.<sup>[19]</sup>

Figure 2 shows optical microscope images of the shape change of a crystal undergoing a phase transition characterized by two parallel phase boundaries. When the crystal was heated to  $176.3\text{ }^{\circ}\text{C}$ , two parallel phase boundaries appeared simultaneously from the two opposite sides (Figure 2a). Upon further heating, these two phase boundaries moved synchronously toward each other and finally stop moving at around  $180.0\text{ }^{\circ}\text{C}$ , leaving a small gap in-between. The reversed phase transition from the  $\beta$  to  $\alpha$ -phase upon cooling starts at around  $177.0\text{ }^{\circ}\text{C}$ , judging from the separation between the two boundaries (Figure 2b). The crystal eventually returned to its original shape at around  $173.4\text{ }^{\circ}\text{C}$ , without any visible damage under the optical microscope.

If the crystal was further heated to a higher temperature ( $10\text{ }^{\circ}\text{C}$  above the phase transition temperature) before cooling, the directions of the in-plane optical axes in the middle of the crystal became permanently changed. The brightness contrast in this part is different from the other parts of the crystal under a polarization optical microscope (Figure S2, Supporting Information), although no clear breakages or surface defects can be observed. This change in birefringence, however, indicates that the lattice in the center was plastically deformed upon over heating.<sup>[20]</sup> Crystals transforming by a single phase boundary did not show any birefringence change even after 30 heating/cooling cycles. The different pathways of this phase transition

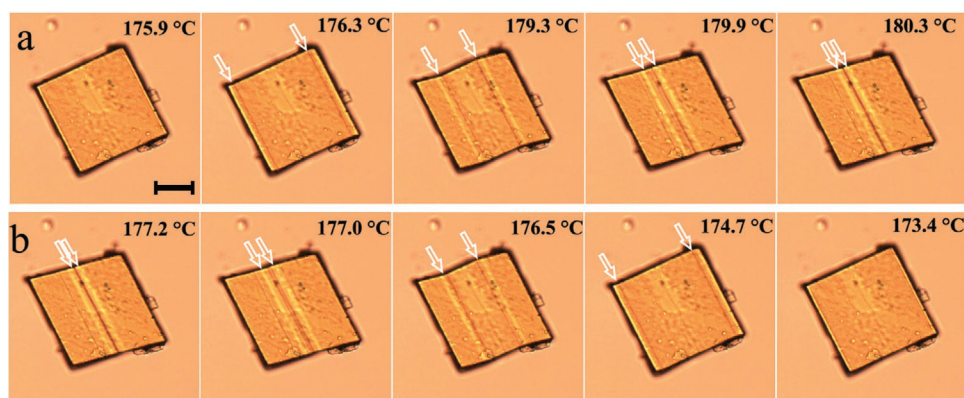


**Figure 2.** A typical single crystal of 4-DBpFO transformed via two parallel phase boundaries upon a) heating and b) cooling. The optical microscope images are extracted from Movie S2, Supporting Information. Scale bar:  $50\text{ }\mu\text{m}$ . Note that: 1) continuously increasing/decreasing the temperature is needed to drive the phase boundaries to move; 2) the metastable crystal shapes during heating are regenerated during cooling; 3) the small gap between the two phase boundaries (the last figure in panel (a)) does not disappear even if the crystal is further heated to  $190\text{ }^{\circ}\text{C}$ ; and 4) the two phase boundaries move at the same speed.



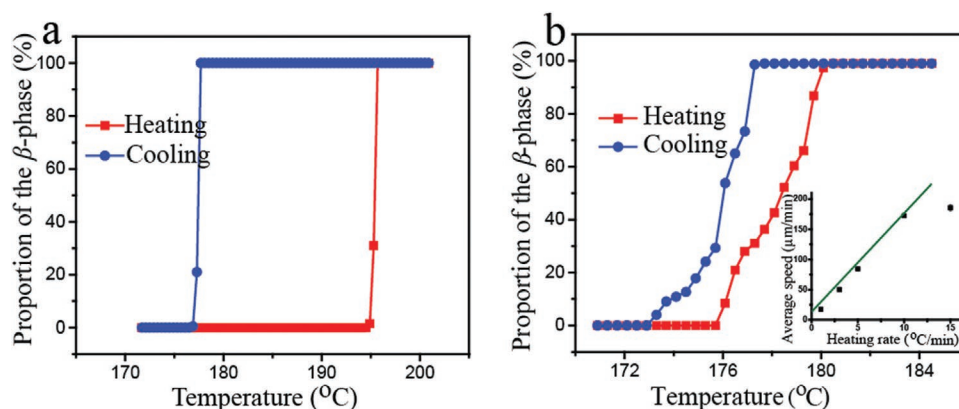


**Figure 3.** Thermal hysteresis loop of phase transition proceeding by a) one single phase boundary and b) two parallel phase boundaries. Proportion of the  $\beta$ -phase is calculated from the microscope images. The inset in (b) shows the average moving speed of the phase boundary at different heating rates, and the green line is a linear fit with a slope of  $16 \mu\text{m } ^\circ\text{C}^{-1}$ .

also result in totally different thermodynamic properties (Figure 3; Figure S3, Supporting Information). In the crystals transformed via parallel phase boundaries, the transition from the  $\alpha$ - to  $\beta$ -phase upon heating (and the reverse from the  $\beta$ - to  $\alpha$ -phase upon cooling) goes gradually (Figure 3b), whereas the transition via a single phase boundary goes abruptly (Figure 3a). In addition, the thermal hysteresis width is much smaller in the crystals transforming via parallel phase boundaries ( $2.0\text{--}3.0^\circ\text{C}$ , Figure 3b) than that in those transforming via a single boundary ( $\approx 18.0^\circ\text{C}$ , Figure 3a). For a  $125 \times 125 \mu\text{m}$  crystal as shown in Figure 2a, we observed a linear relationship between heating rate and phase boundary moving speed with a slope of  $15\text{--}20 \mu\text{m } ^\circ\text{C}^{-1}$  (Figure 3b). This moving speed, corresponding to  $1.3 \mu\text{m s}^{-1}$  at a heating rate of  $5^\circ\text{C min}^{-1}$ , did not show any dependence on the separation of the two boundaries, as for example observed in SCO materials.<sup>[18b]</sup> This is probably due to the fact that the critical distance below which the stored

elastic energy can affect the speed, exceeds the length of our small crystals. The observed speed is also much slower than that at a phase transition via a single phase boundary, which can be as high as  $10 \text{ mm s}^{-1}$ , as shown in Movie S1, Supporting Information.

Thermodynamically, the observed results can be understood as follows. As shown before, the  $\alpha$ - to  $\beta$ -phase transition can be described by a martensitic phase transition, proceeding by a shear deformation in which an in-plane shear force is generated by an anisotropic in-plane lattice expansion<sup>[14]</sup> (Figure 4). For a martensitic transition, the Gibbs free energy difference between the two solid phases consists of two parts<sup>[21]</sup>

$$\Delta G = -\Delta G_{\text{ch}} + \Delta G_{\text{nch}} \quad (1)$$

where  $\Delta G_{\text{ch}}$  and  $\Delta G_{\text{nch}}$  are the chemical and nonchemical contributions to the change of the Gibbs free energy, respectively

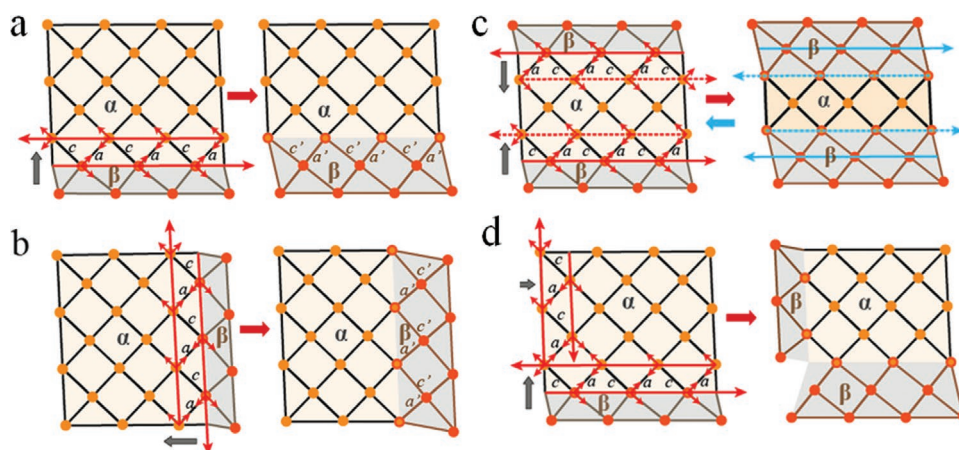


**Figure 4.** Schematic illustration of the in-plane ((010) plane) crystal lattice changes during the structural phase transition at different phase boundary conditions. a, b) Phase transition via a single phase boundary results in two possible orientations of the  $\beta$ -phase, related to the phase boundary directions. The shear force (long red arrows) is caused by the in-plane anisotropic lattice expansion (short red arrows). c) Phase transition via parallel phase boundaries results in a gradual building up of elastic energy in the middle ( $\alpha$ -phase) between the phase boundaries. Two parallel shear forces acting on opposite sides of the crystal can generate an additional shear force (dashed red and blue arrows by heating and cooling, respectively). Note that the extra shear force is toward the opposite direction of the phase transition induced shear deformation, so the extra shear force will result in elastic strain on the middle lattices (marked with bold lines) when the two phase boundaries move toward or away from each other. The bold arrows beside each figure indicate the moving direction of the corresponding phase boundary. d) Phase transition via crossed phase boundaries results in cracking of the crystal due to the crossed shear forces.

(Figure S3, Supporting Information). When a single crystal transforms from the  $\alpha$ -phase to the  $\beta$ -phase, the relative rotation of the phenyl rings results in an in-plane lattice distortion with a shrinking of 9.4% along the crystallographic  $a$ -axis and an expanding of 6.9% along the crystallographic  $c$ -axis, respectively. This cooperative lattice change will generate a shear force on the coherent phase boundary (Figure 4a).<sup>[14]</sup> When a crystal transforms through a single phase boundary, one shear force is generated at that particular phase boundary, driving the crystal transformation to the  $\beta$ -phase through a shear deformation (Figure 4a). The monoclinic  $\beta$ -phase can appear in two different variants, corresponding to two different shear force directions, due to its lower symmetry compared to that of the  $\alpha$ -phase (orthorhombic).<sup>[7]</sup> The direction of this shear force can lead to different crystal orientations (Figure 4a,b) but cannot affect the thermodynamics of the phase transition. On the other hand, as the four side faces of an ideal rhombic crystal are symmetrically equivalent, in principle four phase boundaries can form simultaneously when a high quality  $\alpha$ -phase crystal is uniformly heated. This can lead to complex situations, as illustrated in Figure 4c,d. When the phase boundaries are parallel (Figure 4c), compatible parallel shear forces will be generated on each phase boundary. These parallel shear forces create an additional shear force acting on the  $\alpha$ -phase. Because this extra shear force points towards the opposite direction of the main shear forces on the phase boundaries, it will prevent the movement of the phase boundaries. The extra shear force results in an elastic lattice strain and the building up of elastic energy ( $\Delta G_{\text{elch}}$ ) between the two phase boundaries, similar to what has been demonstrated in shape memory alloys.<sup>[21]</sup> To move the phase transition forward/backward, the chemical energy difference between the two phases needs to be enlarged to balance this stored elastic energy, which can only be achieved by further heating/cooling (Figure S3b, Supporting Information). However, when two phase boundaries cross each other (Figure 4d), the brittle molecular crystals can easily crack (Figure S4, Supporting Information) because of the crossing of the shear forces at the junction of the phase boundaries. This is different from martensitic phase transitions in shape memory alloys that can be elastically deformed.<sup>[19]</sup>

As a consequence of the stored elastic energy between them, parallel phase boundaries can be frozen at a certain position by keeping the temperature fixed, meaning that the intermediate, metastable, shapes of the crystal during the phase transition can be realized by tuning the temperature. For those crystals transforming much more abruptly via a single phase boundary (Figure 3a), the still present but much smaller temperature range between the two phases arises most likely from defects inside the crystals that pin the migration of the phase boundary.<sup>[22]</sup> In principle, for perfect crystals, this phase transition cannot be fixed at intermediate phases, as the chemical energy difference is the only driving force for the phase transition, as observed in many crystals and simulations.<sup>[11,21c]</sup> The difference in the hysteresis widths between Figure 3a,b can now be understood. Because the transformation back from the  $\beta$  to the  $\alpha$ -phase by cooling does not require re-nucleation, the observed thermal hysteresis width is only 2–3 °C (Figure 3b), which is much smaller than those for the crystals transformed via single boundaries (as large as 15–20 °C, Figure 3a). Note that the thermal hystereses are in the range of 10–80 °C for

most of the reported thermosalient crystals (Table 1). Also note that because of the additional shear force between the two phase boundaries, the  $\alpha$ -phase cannot completely transform into the  $\beta$ -phase, even when the crystal is overheated to 190 °C (Figure S5, Supporting Information) where plastic deformation appears (Figure S2, Supporting Information).

The appearance of parallel phase boundaries has important consequences for applications, as the elastic energy stored in-between allows for controllable temperature-dependent shape changes. Since the position of the phase boundaries is only related to the temperature but not to the heating rate (Figure S6, Supporting Information), and the intermediate crystal shapes generated upon heating can be reproduced while cooling, one can easily tune their position in both time and space by a programmed heating/cooling process (Figure 5; Movie S3, Supporting Information). Moreover, the temperature range between the phase transition starting point (176 °C) and finishing point (180 °C) is large enough so that the phase boundary position can be easily tuned with a low heating rate, where the instrumental's response time to the temperature change is negligible. Furthermore, because of the small hysteresis width and the good reversibility, these crystals can be cycled between their two shapes very rapidly. For example, the reversed shape deformation can be repeated three times in 1.2 s without any damage, as shown in Movie S4, Supporting Information. Such a shape-oscillating crystal could be exploited to generate continuously output as a crystalline motor or actuator. Moreover, benefiting from the cooperative molecular movements, the molecular packing in the phase boundaries is not distorted during the phase transition. Therefore, these metastable Shapes can still show waveguiding behavior like a single crystal (Figure S7, Supporting Information). The tunability and reversibility of the change in the crystal shape, together with their efficient solid state fluorescence,<sup>[23]</sup> make these crystals also ideal for the development of thermally controlled flexible organic waveguides, similar to those reported in mechanical induced elastic organic crystals.<sup>[24]</sup>

In many materials, the temperature of the martensitic phase transition will shift after many cycles, resulting in a degradation of their function.<sup>[25]</sup> This change could be much more severe in molecular crystals due to their weak intermolecular forces. However, in 4DBpFO crystals, the phase boundaries move to the same position for a given target temperature, even after 30 cycles (Figure 5). The reproducibility is most likely due to the fact that the phase boundaries are perpendicular to the layered planes of the crystal (Figure S8, Supporting Information).

In summary, we report a fully controllable martensitic phase transition with a very small thermal hysteresis between the  $\alpha$ - and  $\beta$ -phase of a 4DBpFO molecular crystal, when this transition is triggered via two parallel phase boundaries. The two antiparallel shear forces on each phase boundary result in a gradual storage of elastic energy along with the movement of the phase boundaries. Further heating/cooling is needed to enlarge the chemical energy difference to drive the phase boundaries to move forward/backward, endowing these crystals with temperature-dependent shape deformation properties. Controlling the cooperative molecular movements by tuning the temperature allows for a continuous and repetitive movement between the two phases. Moreover, as the  $\alpha$ -phase cannot completely

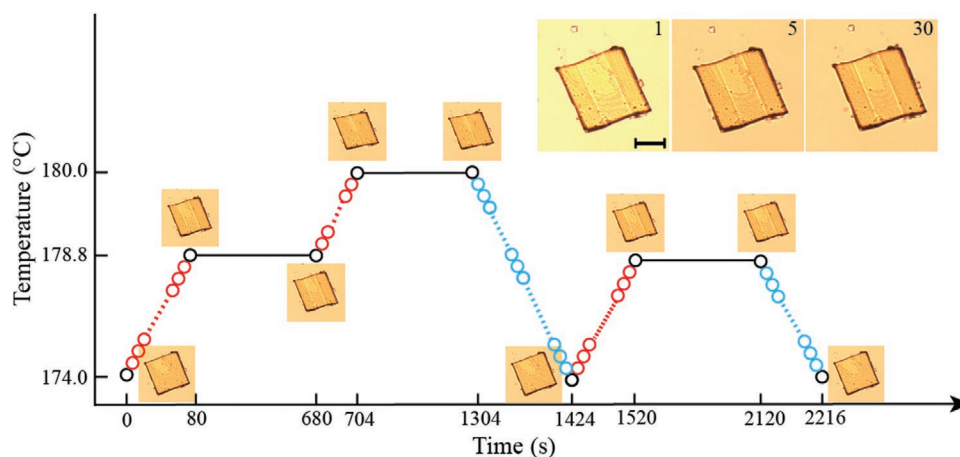


**Figure 5.** Controllable time-varying crystal shape changes along a set of heating/cooling procedures. Each circle represents one crystal shape generated during the phase transition. Red, blue, and black colors represent increase, decrease, and stabilization of the temperature. The microscope images are the corresponding crystal shapes at the temperature of the black circle positions. The heating and cooling rate is 3 °C min<sup>-1</sup>. The inserts show the phase boundaries positions at 178.8 °C during different cycles upon heating. The cycle numbers are shown in the corresponding figures. Scale bar: 50 μm.

transform to the  $\beta$ -phase, the reversed transformation does not require nucleation, leading to a very small thermal hysteresis. Such a greatly reduced thermal hysteresis together with the well-controlled cooperative molecular movements brings these thermomechanical organic crystals a step closer to applications in areas such as organic shape memories, rapidly repeatable actuators, and flexible optical waveguides.

Although this is, as far as we know, the first report of a controllable thermoelastic martensitic phase transition in molecular crystals, similar thermal dynamic behavior has been reported for metallic single crystals with different phase boundary conditions,<sup>[21b]</sup> where two phase boundaries can be selected to form from two sides of a single crystal through nonuniform heating. We believe that the relationship between the phase boundary conditions and the thermodynamic properties of martensitic phase transitions can also be adapted to other thermomechanical molecular crystals. Moreover, different phase boundary conditions may also be one of the reasons that the same kind of molecular crystals displays very different mechanical effects, such as jumping, cracking, rotation, explosion, and deformation.<sup>[26]</sup> While small (smaller than 100 × 100 μm) crystals tend to transform via single phase boundaries, parallel phase boundaries can be much more easily generated in larger crystals (50% possibility in crystals larger than 150 × 150 μm). This is likely due to the fact that smaller crystals have fewer defects than large crystals and are heated more uniformly. Since laser heating-induced phase transitions have also been reported for thermomechanical crystals,<sup>[27]</sup> we speculate that the number of phase boundaries in these crystals may be controlled by making use of nonuniform heating with focused lasers.

## Experimental Section

The detailed synthesis of the 4-DBpFO compound and the crystal growth method can be found in the previous reports.<sup>[14,23]</sup> In short, the  $\alpha$ -phase crystal was grown through a solution-diffusion method by diffusing

heptane into a chloroform solution. Micro-crystals with varying side lengths but smaller than 100 μm were formed after 24 h. Larger single crystals with side lengths larger than 100 μm could be obtained after 2 weeks. Fluorescence images were acquired with a Leica Microsystems DM2500 microscope. Optical microscope images were obtained with a Zeiss Axioplan 2 microscope, equipped with a Media Cybernetics Evolution VF digital camera. A Linkam LTS420 thermal stage and liquid nitrogen cooling system was connected to the microscope to acquire images of the shape change during the phase transition. The crystals can be heated or cooled in the hot stage under nitrogen atmosphere at a rate of 0.1–20 °C min<sup>-1</sup>. To test the fast shape-switching properties (Movie S4, Supporting Information), the single crystal was put on a homemade heating wire and was cooled with an Oxford Cryostream to achieve fast temperature changes.

## Supporting Information

Supporting Information is available from the Wiley Online Library or from the author.

## Acknowledgements

Financial supports from the National Natural Science Foundation of China (NSFC, 21773168), “111 Project” of China (B18030), and the Dutch Research Council (NWO) are gratefully acknowledged. Y.D. acknowledges the financial support from the China Scholarship Council (CSC) and from Radboud University. The authors thank E. Ronde from Radboud University for his technical assistance.

## Conflict of Interest

The authors declare no conflict of interest.

## Data Availability Statement

The data that support the findings of this study are available from the corresponding author upon reasonable request.

## Keywords

crystalline machine, organic crystals, shape memory, structural phase transition

Received: November 5, 2020

Revised: January 25, 2021

Published online: March 12, 2021

- [1] a) C. S. Vogelsberg, M. A. Garcia-Garibay, *Chem. Soc. Rev.* **2012**, 41, 1892; b) T.-A. V. Khuong, J. E. Nunez, C. E. Godinez, M. A. Garcia-Garibay, *Acc. Chem. Res.* **2006**, 39, 413; c) M. A. Garcia-Garibay, *Proc. Natl. Acad. Sci. USA* **2005**, 102, 10771; d) W. R. Browne, B. L. Feringa, in *Nanoscience and Technology: A Collection of Reviews from Nature Journals*, (Ed: P. Rodgers), World Scientific, Singapore **2010**, pp. 79–89; e) W. Danowski, T. van Leeuwen, S. Abdolazadeh, D. Roke, W. R. Browne, S. J. Wezenberg, B. L. Feringa, *Nat. Nanotechnol.* **2019**, 14, 488; f) Z.-S. Yao, M. Mito, T. Kamachi, Y. Shiota, K. Yoshizawa, N. Azuma, Y. Miyazaki, K. Takahashi, K. Zhang, T. Nakanishi, *Nat. Chem.* **2014**, 6, 1079; g) A. Colin-Molina, D. P. Karothu, M. J. Jellen, R. A. Toscano, M. A. GarciaGaribay, P. Naumov, B. Rodríguez-Molina, *Matter* **2019**, 1, 1033.
- [2] a) S. M. Mirvakili, I. W. Hunter, *Adv. Mater.* **2017**, 29, 1604734; b) T. H. Ware, M. E. McConney, J. J. Wie, V. P. Tondiglia, T. J. White, *Science* **2015**, 347, 982; c) T. Xie, *Nature* **2010**, 464, 267; d) Y. Tai, G. Lubineau, Z. Yang, *Adv. Mater.* **2016**, 28, 4665; e) Y. Hu, G. Wu, T. Lan, J. Zhao, Y. Liu, W. Chen, *Adv. Mater.* **2015**, 27, 7867; f) N. Kong, Q. Peng, H. Li, *Adv. Funct. Mater.* **2014**, 24, 7310; g) S. Taccola, F. Greco, E. Sinibaldi, A. Mondini, B. Mazzolai, V. Mattoli, *Adv. Mater.* **2015**, 27, 1668; h) C. Lv, H. Xia, Q. Shi, G. Wang, Y.-S. Wang, Q.-D. Chen, Y.-L. Zhang, L.-Q. Liu, H.-B. Sun, *Adv. Mater. Interfaces* **2017**, 4, 1601002; i) J. Liang, L. Huang, N. Li, Y. Huang, Y. Wu, S. Fang, J. Oh, M. Kozlov, Y. Ma, F. Li, R. Baughman, Y. Chen, *ACS Nano* **2012**, 6, 4508; j) B. Xue, M. Qin, T. Wang, J. Wu, D. Luo, Q. Jiang, Y. Li, Y. Cao, W. Wang, *Adv. Funct. Mater.* **2016**, 26, 9053.
- [3] a) L. Zhu, R. O. Al-Kaysi, C. J. Bardeen, *Angew. Chem., Int. Ed.* **2016**, 55, 7073; b) D. Kitagawa, H. Tsujioka, F. Tong, X. Dong, C. J. Bardeen, S. Kobatake, *J. Am. Chem. Soc.* **2018**, 140, 4208; c) H. Wang, P. Chen, Z. Wu, J. Zhao, J. Sun, R. Lu, *Angew. Chem., Int. Ed.* **2017**, 56, 9463.
- [4] F. Lancia, A. Ryabchun, N. Katsonis, *Nat. Rev. Chem.* **2019**, 3, 536.
- [5] a) R. D. Vale, R. A. Milligan, *Science* **2000**, 288, 88; b) M. G. Van den Heuvel, C. Dekker, *Science* **2007**, 317, 333.
- [6] H. K. D. H. Bhadeshia, in *Encyclopedia of Materials: Science and Technology*, (Eds: K. H. J. Buschow, R. W. Cahn, M. C. Flemings, B. Ilshner, E. J. Kramer, S. Mahajan, P. Veyssière), Elsevier, Oxford **2001**, pp. 5203–5206.
- [7] K. Bhattacharya, R. D. James, *Science* **2005**, 307, 53.
- [8] G. Olson, H. Hartman, *J. Phys., Colloq.* **1982**, 43, C4-855.
- [9] a) P. E. Naumov, S. Chizhik, M. K. Panda, N. K. Nath, E. Boldyreva, *Chem. Rev.* **2015**, 115, 12440; b) D. P. Karothu, J. Weston, I. T. Desta, P. Naumov, *J. Am. Chem. Soc.* **2016**, 138, 13298. c) G. Liu, J. Liu, X. Ye, L. Nie, P. Gu, X. Tao, Q. Zhang, *Angew. Chem., Int. Ed.* **2017**, 56, 198.
- d) M. K. Panda, T. Runčevski, A. Husain, R. E. Dinnebier, P. Naumov, *J. Am. Chem. Soc.* **2015**, 137, 1895. e) H. Chung, D. Dudenko, F. Zhang, G. D'Avino, C. Ruzié, A. Richard, G. Schweicher, J. Cornil, D. Beljonne, Y. Geerts, Y. Diao, *Nat. Commun.* **2018**, 9, 278.
- [10] M. K. Panda, T. Runčevski, S. C. Sahoo, A. A. Belik, N. K. Nath, R. E. Dinnebier, P. Naumov, *Nat. Commun.* **2014**, 5, 4811.
- [11] J. Anwar, S. C. Tumble, J. Kendrick, *J. Am. Chem. Soc.* **2007**, 129, 2542.
- [12] R. Albers, R. Ahluwalia, T. Lookman, A. Saxena, *Comput. Appl. Math.* **2004**, 23, 345.
- [13] G. Zheng, J. Zhang, *J. Phys.: Condens. Matter* **1998**, 10, 275.
- [14] Y. Duan, S. Semin, P. Tinnemans, H. Cuppen, J. Xu, T. Rasing, *Nat. Commun.* **2019**, 10, 4573.
- [15] a) H. Fourati, K. Boukheddaden, *Phys. Rev. B* **2020**, 101, 224101; b) L. Stoleriu, A. Stancu, P. Chakraborty, A. Hauser, C. Enachescu, *J. Appl. Phys.* **2015**, 117, 17B307; c) K. Ridier, G. Molnár, L. Salmon, W. Nicolazzi, A. Bousseksou, *Solid State Sci.* **2017**, 74, A1; d) G. Molnár, M. Mikolasek, K. Ridier, A. Fahs, W. Nicolazzi, A. Bousseksou, *Ann. Phys.* **2019**, 53, 1900076.
- [16] a) M. Sy, R. Traiche, H. Fourati, Y. Singh, F. Varret, K. Boukheddaden, *J. Phys. Chem. C* **2018**, 122, 20952; b) M. Paez-Espejo, M. Sy, K. Boukheddaden, *J. Am. Chem. Soc.* **2018**, 140, 11954.
- [17] a) A. Slimani, F. Varret, K. Boukheddaden, D. Garrot, H. Oubouchou, S. Kaizaki, *Phys. Rev. Lett.* **2013**, 110, 087208; b) C. Chong, A. Slimani, F. Varret, K. Boukheddaden, E. Collet, J.-C. Ameline, R. Bronisz, A. Hauser, *Chem. Phys. Lett.* **2011**, 504, 29.
- [18] a) M. Sy, K. Boukheddaden, *J. Phys. Chem. C* **2020**, 124, 28093; b) M. Sy, F. Varret, K. Boukheddaden, G. Bouchez, J. Marrot, S. Kawata, S. Kaizaki, *Angew. Chem., Int. Ed.* **2014**, 53, 7539.
- [19] A. Stoddart, *Nat. Rev. Mater.* **2019**, 4, 687.
- [20] H. Tang, D. C. Martin, *J. Mater. Sci.* **2003**, 38, 803.
- [21] a) H. Warlimont, L. Delaey, R. V. Krishnan, H. Tas, *J. Mater. Sci.* **1974**, 9, 1545; b) R. Salzbrenner, M. Cohen, *Acta Metall.* **1979**, 27, 739; c) J. Ortin, A. Planes, *Acta Metall.* **1988**, 36, 1873.
- [22] a) H. Zheng, J. B. Rivest, T. A. Miller, B. Sadler, A. Lindenberg, M. F. Toney, L.-W. Wang, C. Kisielowski, A. P. Alivisatos, *Science* **2011**, 333, 206; b) J. Perez-Landazabal, V. Recarte, D. Agosta, V. SanchezAlarcos, R. Leisure, *Phys. Rev. B* **2006**, 73, 224101.
- [23] Y. Duan, C. Ju, G. Yang, E. Fron, E. Coutino-Gonzalez, S. Semin, C. Fan, R. S. Balok, J. Cremers, P. Tinnemans, *Adv. Funct. Mater.* **2016**, 26, 8968.
- [24] a) H. Liu, Z. Lu, Z. Zhang, Y. Wang, H. Zhang, *Angew. Chem., Int. Ed.* **2018**, 57, 8448; b) L. Catalano, D. P. Karothu, S. Schramm, E. Ahmed, R. Rezgui, T. J. Barber, A. Famulari, P. Naumov, *Angew. Chem., Int. Ed.* **2018**, 57, 17254; c) S. Hayashi, S. Yamamoto, D. Takeuchi, Y. Ie, K. Takagi, *Angew. Chem., Int. Ed.* **2018**, 57, 17002.
- [25] Y. Song, X. Chen, V. Dabade, T. W. Shield, R. D. James, *Nature* **2013**, 502, 85.
- [26] a) S. C. Sahoo, S. B. Sinha, M. S. R. N. Kiran, U. Ramamurty, A. F. Dericioglu, C. M. Reddy, P. Naumov, *J. Am. Chem. Soc.* **2013**, 135, 13843; b) S. C. Sahoo, M. K. Panda, N. K. Nath, P. Naumov, *J. Am. Chem. Soc.* **2013**, 135, 12241.
- [27] K.-J. Chen, Y.-C. Tsai, Y. Suzuki, K. Osakada, A. Miura, M. Horie, *Nat. Commun.* **2016**, 7, 13321.